Radio frequency ion source for plasma diagnostics in magnetic fusion experiments

A. A. Ivanov, V. I. Davydenko, and P. P. Deichuli
Budker Institute of Nuclear Physics, Prospect Lavrentieva 11, 630090, Novosibirsk, Russia

A. Kreter
Institut für Plasmaphysik, Forschungszentrum Jülich GmbH, EURATOM Association, 52425 Jülich, Germany[a)]

V. V. Mishagin, A. A. Podminogin, and I. V. Shikhovtsev
Budker Institute of Nuclear Physics, Prospect Lavrentieva 11, 630090, Novosibirsk, Russia

B. Schweer and R. Uhlemann[b)]
Institut für Plasmaphysik, Forschungszentrum Jülich GmbH, EURATOM Association, 52425 Jülich, Germany[a)]

(Received 27 April 2000; accepted for publication 5 July 2000)

Low-divergent quasistationary neutral beams are often applied in modern magnetic fusion devices as a diagnostic tool providing unique information about plasma parameters. The most important requirements of these beams are sufficiently large current and energy of the particles, so that the beam can penetrate to the plasma core. Also the duration of the beams must be long enough, i.e., close to that of a plasma discharge, amounting to at least a few seconds for large fusion devices. We developed a neutral beam injector for plasma diagnostics in the tokamak TEXTOR-94 which is capable of meeting these requirements. The maximum beam energy is 50 keV and the source operated in hydrogen delivers an ion current of up to 2 A with a pulse duration of up to 4 s. The low divergent beam ($\sim 0.5° - 0.6°$) is geometrically focused 4 m downstream from the source having a $1/e$ width of $\sim$ 70 mm at the focal point. The beam can be modulated with a frequency variable up to 500 Hz. The ion source plasma is produced by a radio frequency discharge in hydrogen or helium. The ion beam is extracted by a four-grid system with 163 single holes. The measured beam parameters were compared with those predicted by simulations. © *2000 American Institute of Physics.* [S0034-6748(00)01910-9]

I. INTRODUCTION

Spectroscopy of neutral beam induced radiation is widely used in magnetic fusion devices for diagnostic purposes such as measurement of density and temperature profiles,[1] parameters of plasma turbulence[2] and cross field transport as well as spatial profiles of highly ionized impurities.[1] In particular, by means of a high energy hydrogen (or deuterium) beam it is possible to measure plasma parameters like density and temperature profiles of impurity ions not only in the plasma edge but in the core, as well.

The hydrogen beam energy of 50 keV provides reasonable penetration into the plasma interior in modern plasma physics experiments with a minor plasma radius of 0.5–1 m and an average ion density of $\sim 10^{20}$ m^{-3}. This energy also gives the maximum cross section of the charge exchange of the 7–8 transition of C^{5+} ions being of particular interest for many cases. Only a beam of neutral particles can cross the plasma confining high magnetic field of these experiments without being deflected by the $(v \times B)$ Lorentz force. The estimates suggest that the equivalent neutral beam current incident on the plasma is to be about 1 A or higher to provide reasonable signals in the spectroscopic detection system.[1,3] At the same time the beam power density has to be small enough to prevent significant heating of the plasma which is important for the investigation of ohmic, ion cyclotron and electron cyclotron resonance heated plasmas. A neutral beam injector, even being quite simple in design and capable of meeting the above mentioned requirements, has been developed for spectroscopic measurements of impurities in the plasma of the controlled fusion experiment TEXTOR-94 (torus experiment for technological oriented research), a medium size tokamak with a major radius of $R_0 = 1.75$ m and a plasma radius of $a = 0.46$ m.[1] In fact, the injector can be used in other plasma physics devices with parameters similar to that of TEXTOR-94 and, after modifications that are straightforward, even in larger scale experiments, which are now being planned or constructed.

The ion beam forming system for the plasma diagnostics has to be carefully designed because the beam quality is essential for these applications. The distinguishing feature of the developed injector is that the grids of the ion optical system are inertially cooled, i.e., have no channels for water cooling inside, as it is necessary for high power long pulse ion sources dedicated for plasma heating.[4–7] Due to the limited pulse duration (2–10 s) and long enough intervals between the pulses in present day magnetic fusion facilities, the

[a)]Partner in the Trilateral Euregio Cluster (TEC).
[b)]Electronic mail: r.uhlemann@fz-juelich.de

average thermal power loads on the grids appear to be rather moderate. This allows a much simpler method of cooling if the transverse size of grids is not too large. Essentially, under these conditions the heat capacity of the grids can be made high enough to limit its temperature rise during the pulse to 100–200 K. Subsequently, the heat can be removed from the grids by water cooling from the periphery because of the very moderate time-averaged heat loads ($\sim$100 W). This approach allows us to avoid warping of the precision-machined and carefully aligned grids in long pulse operation and keep their thermo-mechanical deformations at sufficiently low level.

Generally, in practice, diagnostic beam modulation improves the discrimination between the active beam and passive plasma induced signals and thus increases the detection limits. The power supply developed for the injector was designed to provide a modulated beam. In the article the experimental results obtained during the injector testing are presented. In the following sections the description of the radio frequency (rf) ion source is given together with a brief description of the general layout of the diagnostic neutral beam injector that incorporates the ion source. Section IV is devoted to the results of the ion source tests. The results are discussed in the last section in which the future development of the source is also outlined.

II. INJECTOR BEAMLINE

The developed ion source is based on a rf induced plasma discharge.[8] The neutral beam is provided by extraction of charged ions from the rf-driven plasma, their acceleration to the desired energy and subsequent neutralization by charge exchange with a gas target in the neutralizer tube. Then the neutral beam is injected through the opened gate valve and duct structure into the fusion plasma. A retractable calorimeter for beam profile and position measurements is available at the exit of the injector tank. A profile scraper for controlling the vertical beam size is located inside the duct tube. In Fig. 1 the general layout of the diagnostic neutral beam injector is given which incorporates the rf driven ion source on the left and all required systems for the beam control and measurements. On the right the cross section of TEXTOR-94 is shown with the plasma center R_0. The focal point of the diagnostic beam (shaded) is at 4 m distance from the ion source and close to the plasma center. Figure 1 includes the water cooled structures, i.e., neutralizer, ion deflection magnet, residual ion dump, retractable calorimeter, as well as vacuum and cryo pumps and other components which are housed inside or at the cylindrical vacuum tank. The neutralizer tube serves to convert the primary ion beam into an atomic one. Gas is partly supplied to the neutralizer by gas flow from the discharge chamber, the remainder, to supply a sufficient gas target, is sent into the neutralizer through a manifold by making use of a pulsed gas valve. A bending magnet and residual ion dump are placed inside the vacuum vessel on a special servicing platform. The bending magnet deflects the remaining ions of the beam by about 20° (for full energy ions) in the horizontal plane on a funnel-shaped positive ion dump.

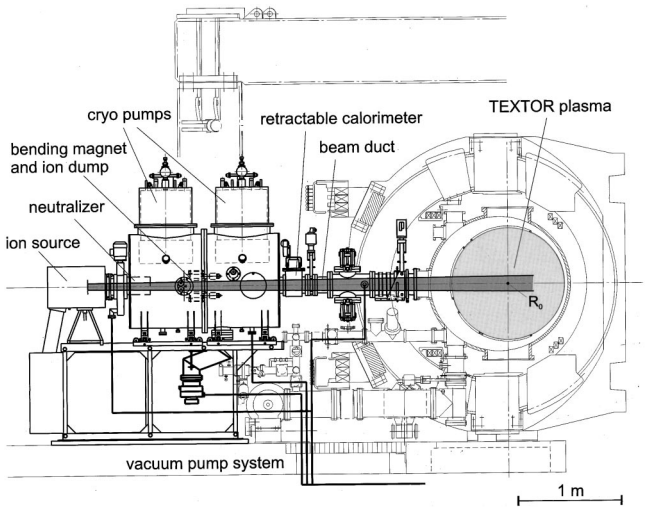

FIG. 1. Diagnostic neutral beam injector setup at TEXTOR-94. The particle beam (shaded) leaves the ion source extraction system on the left and passes through the neutralizer tube and vacuum tank with the LHe cryo pumps and beam duct into the TEXTOR plasma. The focal point (close to plasma center R_0) is given by the curvature of the extraction system. The beam divergence is related to the space charge. Remaining ions are swept out in the horizontal plane by the bending magnet onto the ion dump. For profile measurements a retractable beam calorimeter can be moved into the beam line axis.

The vacuum system is comprised of two liquid-helium cryogenic pumps and one turbo-molecular pump with 250 l/s pumping speed, which is used for initial pump down of the injector vessel and during regeneration of the cryogenic pumps. Each cryo pump installed on the top of the injector tank has a measured hydrogen pumping speed of 24 000 l/s in the molecular flow regime.

To meet the requirements of the diagnostics at TEXTOR-94, the basic version of the injector was designed for a particle energy of up to 50 keV, an equivalent atomic beam current of up to 1 A in hydrogen and a pulse duration of up to 10 s with 500 Hz modulation, i.e., 5 s beam-on time.

III. ION SOURCE

A. Plasma discharge

The injector ion source comprises a rf plasma source feeding a multi-aperture electrostatic accelerator. The plasma source consists basically of a vacuum-tight cylindrical alumina ceramic chamber of 105 mm inner diameter and 95 mm length, and an external rf coil (Fig. 2). For the ion source, an ion current density of 100–130 mA/cm^2 was chosen. The emitter plasma is produced by an inductively excited rf discharge in hydrogen or helium. The external rf coil is made of six turns of six-in-parallel copper wires wound on a Teflon frame that are fed by rf current with a frequency of 4.65 MHz from an amplifier with up to 10 kW variable output power. The rf coil is connected to the amplifier via an insulating transformer, so that the rf amplifier can be operated on ground potential. Typically, to provide the required current density of 130 mA/cm^2 about 2.5 kW of rf power is to be coupled into the plasma. The position of the rf antenna relative to the plasma grid flange was optimized for an efficient plasma production. It was also found that capacitive coupling of the rf power is essential for the efficiency of plasma pro-

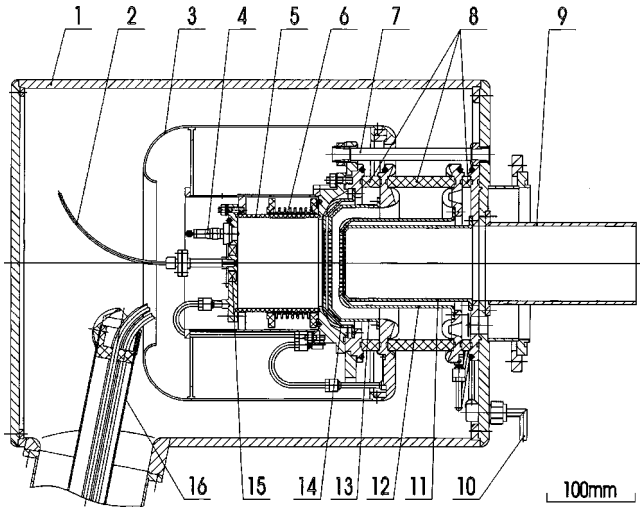

FIG. 2. Radio frequency-discharge ion source: 1-soft metal case; 2-gas feeding capillary tube; 3-inner magnetic shield; 4-trigger electrode; 5-ceramic wall; 6-rf antenna; 7-pull stud (insulator); 8-ceramic spacers; 9-neutralizer tube; 10-grid cooling manifold; 11-grounded grid; 12 acceleration grid; 13-extraction grid; 14-plasma grid (each grid incl. grid holder); 15-permanent magnets; 16-coaxial feedthrough

duction in the rf plasma box. Namely, in special experiments, a cylindrical Faraday shield with axial cuts was mounted to prevent plasma interaction with the ceramic chamber walls. For this arrangement the negative effect of the eddy currents on the penetration of the alternating axial magnetic and azimuthal electric field is negligible. However, it turned out that the Faraday shield considerably reduces the power efficiency, so that 30%–40% more rf power is required to achieve the same current density as without the shield. This reduction is attributed to the electrostatic shielding of the rf coil.

The copper backplate of the plasma source vacuum vessel has water channels for active cooling. The ceramic plasma chamber is vacuum sealed from both ends with indium O-ring seals that allow for effective heat conduction to the backplate and front side flange which are both water cooled. A thermocouple monitoring the surface temperature of the ceramic chamber revealed temperature rises at the tube center of less than 50 K under conditions of 10 s operation at nominal rf power.

The gas is introduced at the backplate by a pulsed gas valve through a flexible capillary tube of 0.5 mm inner diameter and about 150 mm length which simultaneously provides electrical insulation of the valve, installed on the grounded flange, from the plasma source. During the beam extraction the gas pressure inside this capillary tube should be high enough to prevent electrical breakdowns along the tube. To avoid these breakdowns, the gas pressure inside the capillary tube is controlled for the given gas flow rate by a special diaphragm with a microhole at the tube outlet. For 1.5–2 A extracted current the gas flow rate for hydrogen is set to 2 mbar l/s. The timing sequence of the gas pulse, rf voltage application, plasma ignition triggering pulse and extraction high voltage is discussed in Sec. IV A.

The discharge is initiated by applying a high voltage pulse between the trigger electrode (Fig. 2) and discharge

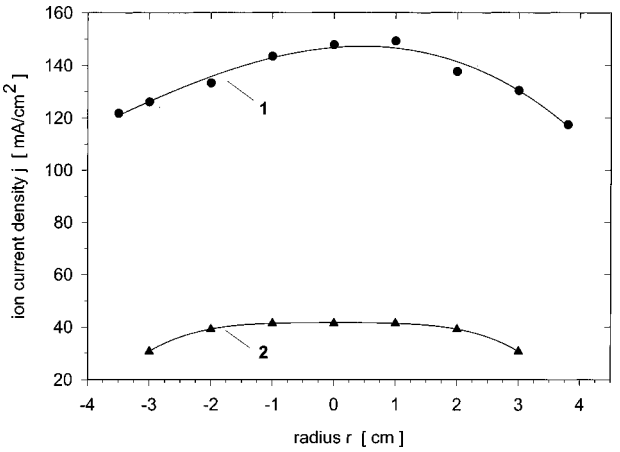

FIG. 3. Typical radial ion current density profile of rf plasma discharge: 1-discharge in hydrogen, 2-helium, for the same 2.5 kW absorbed rf power.

chamber rear flange at which the trigger is mounted. Voltage is applied to the trigger simultaneously with the rf power. Without the trigger being fired, the ignition of the discharge becomes unstable: it is not initiated at all or may start with an unpredictable delay after rf voltage is applied, especially if the rf voltage on the coil is less than 1.5 kV. By using this triggering technique we are able to run the rf source reliably in a wide range of operated rf power and gas pressure. To improve the particle confinement in the source, two NdFeB permanent magnets are installed at the backplate. A typical ion current density profile measured in the plane of the first (plasma) grid is shown in Fig. 3 for 2.5 kW of rf power coupled into the plasma which corresponds to about 2 A extracted ion current for hydrogen. The figure shows that the ion current density is sloping down by about 20% from the center towards the edge of the plasma grid. This provides $\pm 10\%$ homogeneity over the extraction region diameter of 72 mm which is sufficient for precision formation of the ion beam. The ion current density was found to change almost linearly with the rf power coupled into the plasma (see Fig. 4). The homogeneity of the plasma remains almost the same in the total range of rf power studied.

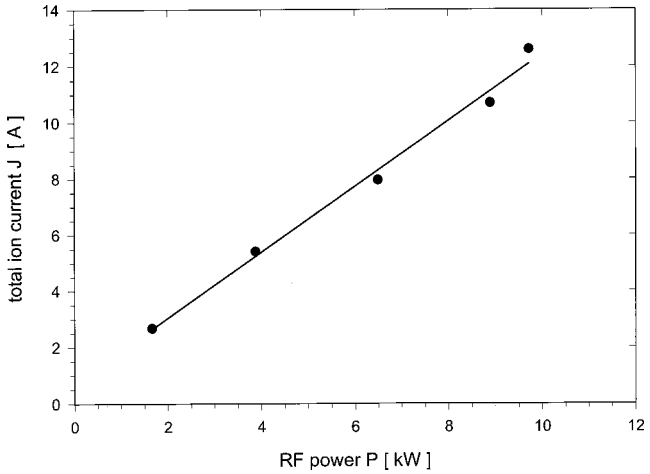

FIG. 4. Total ion current inside the extraction region (72 mm in diameter) vs rf power coupled into the plasma.

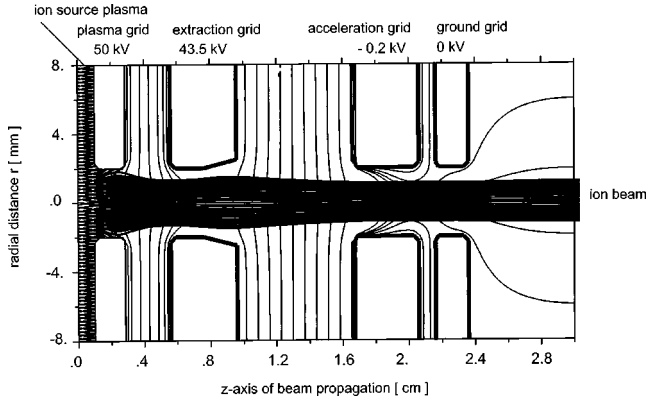

FIG. 5. Calculated ion beam trajectories and equipotential lines (vertical) of optimized grid version at current density of $j=130$ mA/cm^2, i.e., $J^+_{\text{extr}}=1.7-1.8$ A, beam divergence $\theta_{\text{rms}}=0.6°$, species mix $H^+:H_2^+:H_3^+=71.5:13:15.5\%$ (AXCEL code, $T_i/T_e=1/5$ eV, $V_p=40$ V). Grid voltages $U_1/U_2/U_3/U_4$ are 50/44.5/−0.2/0 kV.

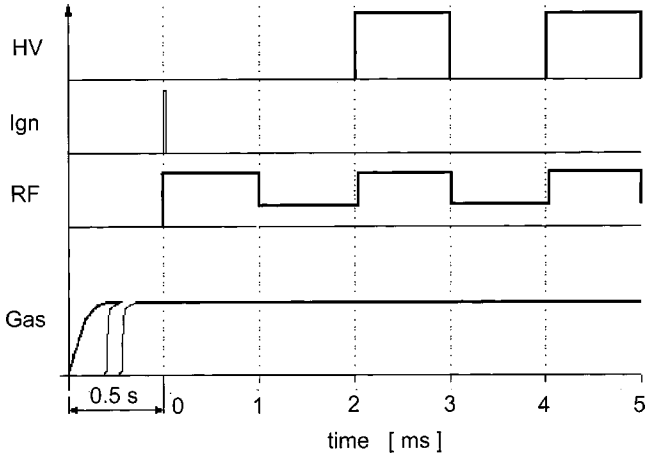

FIG. 6. Schematic of the typical wave forms of gas flow rate, rf power, voltage on triggering electrode (Ign.), and extraction voltage (HV) during ion source operation with 500 Hz modulation.

B. Acceleration grids

The accelerator consists of a set of four nested grids with the 163 circular apertures 4 mm in diameter.[8] The apertures are configured in a hexagonal pattern with a distance separation of 5 mm. The distinctive feature of the ion source is that in order to simplify fabrication of the injector, a thermal inertia-type ion optical system with ''thick'' electrodes is used. To limit the temperature rise of the grids to a tolerable value the extraction and acceleration grid are made of 4-mm-thick molybdenum. The thickness of the plasma grid and ground grid is 2 mm (Fig. 5). The grids are mounted on the water-cooled flanges enabling the full heat removal from pulse to pulse as well as partial heat removal during the injection pulse.[9] In order to focus the beam onto the desired point inside the plasma, the grids are formed to spherical segments with the desired curvature radius of 4 m. Numerical simulations of the grid behavior under the expected heat loads have suggested that the grid temperature could rise by max. 200–250 K at a pulse length of 10 s which leads to still tolerable grid deformations.[9]

The geometry of the beam electrodes was optimized to obtain appropriate angular divergence of the beam.[10] During the simulations the key issues for this type of ion optical system were addressed, namely, whether the divergence of the single beamlet emerging from the thick grid apertures can be made small enough and whether the source grid deformations during long pulse operation are low enough to ensure precise beam formation and focusing. It is rather clear that an increase in the electrode thickness may deteriorate the divergence of elementary beams because inside the holes with a length comparable with the hole diameter the transverse focusing fields of electrodes are screened down. The ions passing through the electrodes will therefore gain an undesired additional angular spread under action of the space charge field. After extensive simulation runs with the two-dimensional computer code AXCEL,[10,11] the four-electrode ion optical system version was accepted in which, in order to provide the accurate beam formation at the initial stage, on the output side of the plasma electrode there is a conical cut with an angle of 60° that is close to the Pierce angle. The shape of the holes in other grids and the potentials on the grids were also optimized, so that in the simulations a beamlet divergence less than 0.6° was obtained. Figure 5 shows the electrode geometry, electrode voltages, and ion trajectories in the optimized version of the ion optical system. In this version the gaps between the plasma grid, extraction grid and acceleration grid are 2.6 and 7 mm, correspondingly.

The effect of electrode heating on the beam quality was also investigated.[9,10] The estimations show that these 4-mm-thick grids are capable of operating for at least 5 s pulses at full power (that corresponds to 10 s pulses with modulation) without significant deterioration of the beam quality. In the next section the results of the experimental testing of the ion source are presented which confirm the simulations results. Also it is worthwhile to note that the ion optical system with thick electrodes could also benefit from smaller admissible negative biasing of the acceleration grid. As a matter of fact, simulations have shown, and it was further proven by direct measurements, that the negative potential barrier for back streaming electrons is established on the axis of the hole in the acceleration grid for a voltage on the grid as small as −200 V. This is to be considered as an advantage of the suggested grid design.

IV. EXPERIMENTAL RESULTS

A. Electrical wave forms

The rf power coupled to the plasma box and extraction high voltage are turned on according to the temporal sequence shown in Fig. 6. First, the gas valve is turned on starting to introduce the gas into the capillary tube connected to the plasma box. After the required gas flow rate from the tube is established, that typically requires 0.2–1 s depending upon the characteristics of the valve used and length of the capillary tube, rf voltage is applied to the coil. Once the rf voltage is applied, the triggering pulse follows to initiate the discharge.

Our investigation of modulated beam formation commenced with modulation of the extraction voltage at constant current density in the plasma source. We found, however,

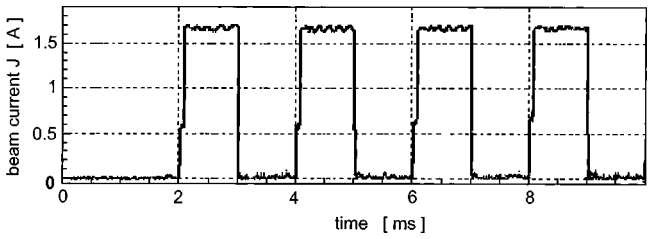

FIG. 7. Oscilloscope display of the extracted ion current with 500 Hz modulation.

that in this case the beam current density is limited to about 50 mA/cm^2 (for 30–50 kV energy) by breakdowns of high voltage (HV) applied between the plasma and extraction grid. For higher current densities it was observed that these HV breakdowns occurred during voltage increase after a pause between individual pulses or after voltage reapplication following a high voltage breakdown. Having experienced difficulty with these breakdowns, we started to raise up the current density in the plasma source with ~ 100 μs delay from high voltage application. Namely, after the discharge has been initiated, the rf voltage was decreased to a smaller level which has been chosen as a compromise between two requirements. First the discharge has to be steadily sustained at this small level of rf power, and, simultaneously, it should be small enough to allow a high voltage application to the grids without immediate flashover when the beam starts or after ion optical system recovery following a high voltage breakdown.

A typical wave form of the extracted current is shown in Fig. 7. It can be seen that during the ramp up of the extracted current there is a step change that corresponds to the above mentioned transition from lower to higher rf power.

B. Beam parameters and beam diagnostic

The beam profiles were measured by an array of secondary emission detectors (SEDs) near the focal plane at a distance of 4.1 m downstream from the ion source on the test stand in Novosibirsk and, alternatively, by a segmented retractable calorimeter located 2.2 m from the ion source after installation of the injector at TEXTOR-94 in Jülich. To infer the beam divergence from the measured profiles, the beam profile at the two positions has been calculated as a function of beamlet divergence and accelerator focal length. It was assumed that the grid curvature, determining the focal length, is uniform and beamlet divergence distribution is of Gaussian type. Considering that the number of beamlets (163) is quite large, the local current density in the beam at a distance z can be evaluated by using a simple analytical approximation. Namely, we assumed that the ion current density is constant (and equal to an averaged one) over the circular plasma emitter and at each point of the emitter the divergence θ is equal to that in the beamlet. By Eq. (1) the local beam current density j in each point with radius r at any distance z from the source can then be calculated as

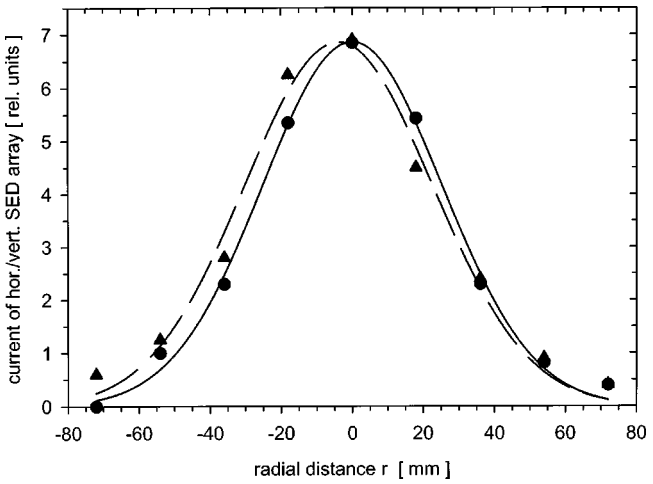

FIG. 8. Horizontal (●●●, —) and vertical (▲▲▲,- - - -) beam profiles at 50 kV, 1.7 A, 1 s in the focal plane in 4.1 m distance measured with the SED array. The $1/e$-beam widths are 71/75 mm horiz./vertical and deviations of the beam center from the duct axis are 0.1/−3.8 mm, respectively, found by Gaussian fits of the measurements.

$$j(r,z) = 2J/\pi a^2 z^2 \theta^2 \cdot e^{-r^2/(\theta \cdot z)^2} \times \int_0^a e^{-\eta^2/(\theta \cdot z^*)^2} I_0(2\eta r/zz^*\theta^2)\, \eta d\eta \qquad (1)$$

with

$$\frac{1}{z^*} = \frac{1}{z} + \frac{1}{R}, \qquad (2)$$

where J is the total beam current, a is the initial beam radius, and R is the curvature radius of grids or focal length of the accelerator. This expression is obtained by summing up the contributions to the current density $j(r,z)$ from the elements of the emitting surface. The integration in Eq. (1) is performed in cylindrical coordinates where the integrand corresponds to the contribution of an elementary ring with radius η and width $d\eta$ to the local current density in the beam. In the data analysis the PADET[12] computer code, a more comprehensive model that sums up the contribution of each individual beamlet, was also used.

Since the SED array was located near the focal point, the $1/e$-beam intensity radius at this position is directly determined by the divergence θ as $R \times \theta$. The results of the calorimetric measurements reasonably coincide with the SED data. However, when the beam duration exceeds 0.5–1 s, the direct measurements of the beam profile by the SEDs becomes unreliable due to an uncertainty provided by generation of a dense secondary plasma near the detector surface. Therefore for longer beam pulses the divergence was derived from the calorimetric measurements. The beam profiles, as seen by the SED array, are shown in Fig. 8 together with their Gaussian fits.

The given profiles correspond to the beam divergence characterized by the half-width at $1/e$ level of about $\pm$ 0.5° (measured for 50 keV beam energy). The V-shaped dependence of the angular divergence upon the beam current and voltage of the extraction electrode (Fig. 9), i.e., perveance scans, have been obtained near the focal length at 4.1 m

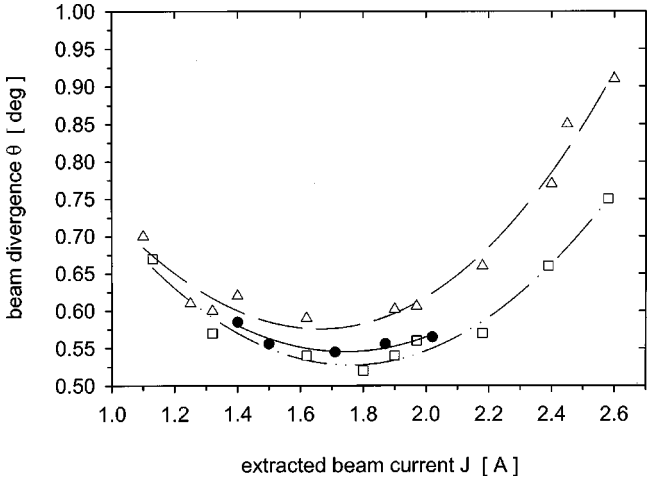

FIG. 9. Measured beam divergence vs beam current at 50 kV, 1 s for the extraction grid (g2) voltage 6.5 kV (lower curve) and 6.75 kV (upper curve). Circles stand for calorimetric data, triangles and rectangles are SED array data near the focal plane at 4.1 m.

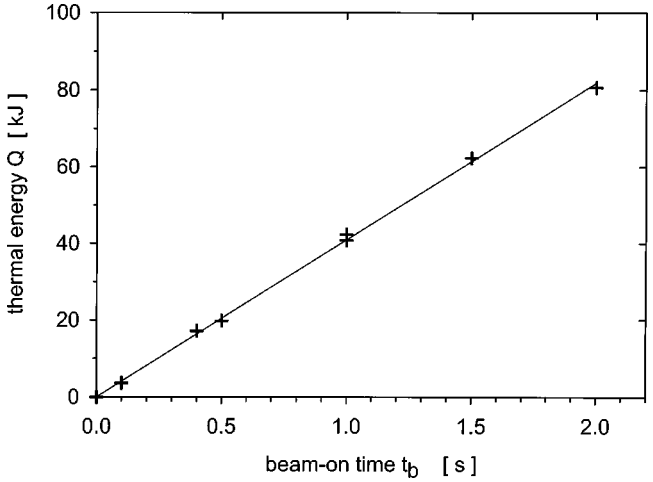

FIG. 11. Thermal energy deposited on the calorimeter beam target at 50 kV, 1.7 A vs beam-on time t_b in 4.1 m distance.

distance with the SEDs and the calorimeter. The potential difference between the plasma and extraction electrode (grid2) was varied from 5.5 to 7 kV to obtain minimal beam divergence.

After the diagnostic beam injector was built up and commissioned at TEXTOR-94 the beam profiles were measured on the retractable beam calorimeter (Fig. 1) in the beam line at 2.2 m distance from the ion source grids. At 50 kV, H_2, and 2 s modulated pulse length (1 s beam-on time) the beam current was varied from 1.4 to 2.1 A. The neutral beam profiles were measured with eight thermocouples in horizontal and vertical direction, respectively. The variation of the 1/e width of the profiles is shown in Fig. 10. The perveance matched beam current at minimum beam width, i.e., divergence, is about 1.7 A for the horizontal and vertical direction. The working range of the ion source is also marked in Fig. 10 where the beam width is close to its minimum and beam losses in the beam line are smallest. Within the thermal measuring accuracy both beam widths can be assumed as nearly equal, i.e., the beam is of circular cross section, as expected from the grid hole position matrix. Comparison of the measured minimum beam width of 4.1 cm with the beamline simulation code PADET[12] gives a beam divergence of $\theta \approx \pm 0.5°$ which is in good agreement with the results of Fig. 9 obtained near the focal length.

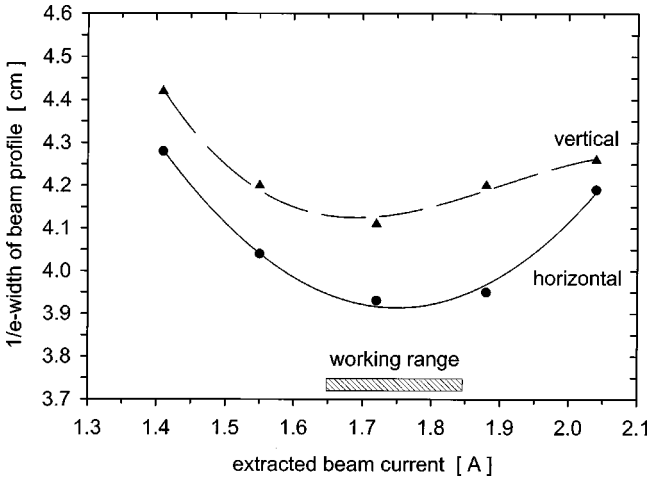

FIG. 10. Perveance scan at 50 kV, H_2 , 2 s, neutral beam on beam calorimeter in 2.2 m distance (shot No. 33001-06). Measured horizontal (●●●) and vertical (▲▲▲) beam width vs extracted beam current.

Experimental tests indicate that the grids are capable of handling the pulsed thermal load when operated at 50 kV with an extracted ion current of, at least, 1.7 A for 4 s every 4 min, i.e., a duty cycle of about 1.5% for cooling. This was confirmed at the test stand in BINP, Novosibirsk, by special measurements of the hydrogen beam energy, deposited on a stationary calorimeter located 4.5 m from the source, for different pulse duration when the grid temperature rises may be significant. The diameter of the calorimeter target was 10 cm. The obtained dependence for 50 keV beams with 1.7 A extracted ion current without modulation (that corresponds to max. 4 s modulated beam) is shown in Fig. 11. The energy deposited on the calorimeter target grows linearly with beam on time, so one can conclude that the beam characteristics do not change.

The experimental results of the beam divergence and value of optimal extraction (grid 2) voltage were also found to be in reasonable agreement with the AXCEL code simulation of the beam formation in the elementary cell of the ion optical system.[10]

The ion species composition has been investigated for a 50 keV hydrogen beam. The beam was analyzed by a magnetic mass spectrometer located $\sim$ 4 m from the source. The mass analysis of the ion beam molecular fractions indicates that H^+, H_2^+, and H_3^+ species percentages are 71.5%, 13%, and 15.5% , respectively, when the ion source is operated at 1.9 A of beam current.

In principle, helium beam formation in the ion source does not differ much from the hydrogen beam formation. Switching to He beam production similarly needs high enough spatial uniformity of ion current density over the plasma emitter. The result obtained for the rf discharge in helium is good as Fig. 3 shows. Of course, for accurate helium beam formation the current density is to be reduced

TABLE I. Characteristic rf ion source data.

Parameter	H_2	He
Beam energy	50 keV	
Ion/neutral beam current	1.7 / 1 A	1 / 0.8 A
Operated pulse length	4 s (modulat.)	1.5 s (continuous)
Max. pulse length	10 s	10 s
Duty cycle (pulse/pause)	1.5%	
rf power to source plasma at 4.65 MHz	2.3 kW	2.5 kW
Current density near grid	100–130 mA/cm^2	50 mA/cm^2
Current density homogeneity	±10%	
Ion source material	Alumina ceramic	
Plasma chamber dimensions	∅ 105× 95 mm, cylindrical	
Grid material	molybdenum	
No. of grid holes	163	
Grid diameter	72 mm	
Grid thickness (plasma/ extract./accel./ground grid)	2/4/4/2 mm	
Grid hole diameter	4 mm	
Gap width	2.6/7/1 mm	
Grid voltages (g1/g2/g3/g4)	50/43.5/−0.2/0 kV	
Focal length	4 m	
Ion species mix (H^+: H_2^+ : H_3^+)	71.5:13:15.5%	100% He^+
Neutralization efficiency	~60%	~80%
1/*e* beam width in 2.2 / 4.1 m	40 / 73 mm	
Max. neutral beam current		
Density in 2.2/4.1 m distance	50 (measured)/15 mA/cm^2 (PADET code)	
Exp. neutral beam divergence θ	~0.5°	~ 0.6°
Theor. single beamlet diverg. θ_{rms}	0.6° (AXCEL code)	
Gas flow rate into source	2 mbar l/s	1.6 mbar l/s
LHe cryo pump speed	2 × 24 000 l/s	
Beam line pressure (with beam)	~5×10^{-5} mbar	

twice in accordance with the mass dependence given by the Child–Langmuir law.

The typical He gas flow rate into the rf discharge with ion current density of ~60 mA/cm^2 was 1.6 mbar l/s. In a reasonable agreement with the results of the ion profile measurements of the hydrogen discharge, helium beams with a current of 1 A at 50 keV energy were extracted. An integral angular divergence of 0.6° of the formed He beam focused at 4 m distance was measured which is reasonably close to the divergence of the hydrogen beam.

V. DISCUSSION AND OUTLOOK

Experimental tests of the ion source show that the ion optical system is capable of handling the pulsed thermal load when operated at 50 kV, 1.7 A, 4 s with a duty cycle of about 1.5%. The beam is focused at a distance of 4 m from the source where the intensity profile has a 1/e diameter of ~70–80 mm. Independent beam profile measurements at 2.2 and 4.1 m distance from the ion source give in good agreement a beam divergence of $\theta = \pm$ 0.5°. The beam is modulated with 500 Hz frequency or can be ''super'' modulated by superimposing additional arbitrary modulation with a time dependence provided by external control. The discussed ion source data are summarized in Table I.

The adopted ion optical system with thick electrodes, besides its low cost and relatively simple fabrication, has several advantages as compared to those with internal cooling channels, namely, higher transparency and possibility of using molybdenum grids with high electrical strength. The impossibility of developing a water leak in the grids is also an important issue contributing significantly to the overall reliability of the ion source.

The present ion source was designed for a maximum pulse length of 10 s with modulation and it is now routinely operated at TEXTOR-94 for 4 s. However, durability of the source operated with 10 s pulse length and longer is still an open question because only a limited number of single pulses longer than 4 s have been fired so far. Modifications of the grids may be desirable or necessary to ensure stable source operation for longer pulses and transition to the dc regime.

Increasing the extracted ion current beyond 2 A is also considered to be an attractive option to meet the demands in other fusion experiments. The principle design issue involved in further increase of pulse length and ion current is the realization of a more effective heat removal from the grids during beam-on phase. Currently, a solution is considered that suggests grid segmentation with introducing water channels going in-between the segments. This would limit the temperature of a segment to ~100 °C even for continuous operation of the source with the present power loads to the electrodes. This approach allows only an insignificant reduction of the grid transparency and to apply a simpler and reliable method compared to embedding the cooling channels in the massive body of the grid using the common milling technique with electrodeposition (galvanizing) of copper or tight welding.

ACKNOWLEDGMENTS

The authors would like to thank V. Savkin and I. Averboukh from the Budker Institute, Novosibirsk, for the development of the power supplies and for their technical assistance throughout this work. Planning and skillful technical work of B. Granderath, G. Gutzmann, U. Habrichs, N. Sandri and H. Schmitz from IPP Jülich during implantation of the injector in the subsystems of TEXTOR-94 is gratefully acknowledged. This work was partially supported by WTZ (Bilateral Scientific and Technological Collaboration) under Project No. RUS-567-99.

[1] E. Hintz and B. Schweer, Plasma Phys. Controlled Fusion **37**, 87 (1995).
[2] M. Jakubovski, R. Fonk, J. S. Kim, and G. McKee, Rev. Sci. Instrum. **70**, 874 (1998).
[3] L. Carraro, M. E. Puatti, F. Sattin, P. Scarin, and M. Valisa, Rev. Sci. Instrum. **70**, 861 (1999).
[4] E. Speth *et al.*, Fusion Eng. Des. **46**, 383 (1999).
[5] M. M. Menon *et al.*, Rev. Sci. Instrum. **56**, 242 (1985).
[6] M. C. Vella, W. S. Cooper, P. A. Pincosy, R. V. Pyle, P. D. Weber, and R. P. Wells, Rev. Sci. Instrum. **59**, 2357 (1988).
[7] Y. Ohara, M. Akiba, Y. Arakawa, Y. Okumura, and J. Sakuraba, J. Appl. Phys. **51**, 3614 (1980).
[8] V. I. Davydenko *et al.*, *Proceedings of the 18th Symposium on Fusion Technology (SOFT), Karlsruhe, Germany, 1994* (Elsevier, Amsterdam, 1995), p. 601.
[9] A. Beklemishev, V. Davydenko, A. Ivanov, and A. Podyminogin, Rev. Sci. Instrum. **69**, 2007 (1998).
[10] V. I. Davydenko, A. A. Ivanov, A. I. Rogozin, and R. Uhlemann, Rev. Sci. Instrum. **68**, 1418 (1997).
[11] *The Physics and Technology of Ion Sources*, edited by Ian G. Brown (Wiley, New York, 1980), Chap. 3.
[12] R. Uhlemann and J. Ongena, Fusion Technol. **35**, 42 (1999).